Heat Pipe Science and Technology: An International Journal 6(3–4) 135–153 (2015)

MICROREACTORS FOR BIODIESEL SYNTHESIS: DESIGN, FABRICATION, AND CHARACTERIZATION

Carolina P. Naveira-Cotta,[1,*] Christopher P. Tostado,[1] Jose Martim Costa, Jr.,[2] & Jeziel S. Nunes[3]

[1]*Laboratory of Nano & Microfluidics and Microssitems – LabMEMS Department of Mechanical Engineering-PEM & Department of Nanoengineering-PENT, Federal University of Rio de Janeiro-UFRJ, Rio de Janeiro-RJ, Brazil, CEP: 21941-914, Cx. Postal 68529*

[2]*Federal Instituto Sertão Pernambucano – Campus Serra Talhada Rua Irineu Magalhães, 985, AABB CEP: 56912-140*

[3]*Federal Center of Technological Education-CEFET Mechanical Engineering Coordination Rio de Janeiro, Brazil, CEP 23810.000*

*Address all correspondence to: C. P. Naviera-Cotta; E-mail: carolina@mecanica.coppe.ufrj.br

The present work describes microreactors for biodiesel continuous synthesis that have been designed, fabricated, characterized, and aimed at achieving a reproducible microfluidic device to compose a modular portable biodiesel production demonstration unit. A straightforward method is presented for the microfabrication and sealing of the microfluidic device that performs the role of a microreactor for biodiesel synthesis, built on a brass metal base and sealed with either a metal cover or a glass cover for easy microscopic observation of two-phase flow patterns. The microfluidic device contains a Y-junction squared microchannel architecture with width and depth of 400 μm. Microchannels were engraved using a micromilling technique and sealed either by welding, with tin as an additional material, in the case of the all metal device, or by using an epoxy glue, which served as an adhesive to seal a metal–glass device. The quality of the metal-on-metal seal was examined using microscopic analysis of multiple cross sections of the device, whereas the quality of the metal-on-glass seal was analyzed via direct visual inspection of flows within the device using an optical microscope to verify the existence or absence of leaks. An experimental setup was then built to carry out biodiesel synthesis in the metal–metal microreactor, using soybean oil of food grade, absolute ethanol, and sodium hydroxide, NaOH, as a catalyst for the reaction. For a molar ratio ethanol/oil 20:1, a quantity of NaOH catalyst of 1.0 wt.% at a controlled temperature of 47.5°C, it was possible to achieve a yield of fatty acids ethyl esters of 87.2% with 98% of triglyceride converted, for a residence time of 10 min. The experimental analysis confirms the applicability potential of the designed microreactor in the synthesis proposed.

KEY WORDS: *microreactors, biodiesel synthesis, microfabrication, microscopic characterization, reactive flow*

1. INTRODUCTION

In recent years, microfluidic devices have been of great interest to various industries including pharmaceutical (Chen et al., 2015), petrochemical (Nilsson et al., 2013), cosmetic, and food ones (Chen et al., 2014), as well as to various academic fields, such as biomedical research, because of their versatility and ability to serve as effective platforms for studying different applications and phenomena, such as controlled drug delivery (Kong et al., 2014), DNA analysis (Le Roux et al., 2014), novel interfacial and flow phenomena (Xu et al., 2014), and the development of microunit operations such as micro heat exchangers, among several other purposes, to cool high concentration photovoltaic cells (Correa et al., 2013; Guerrieri and Naveira-Cotta, 2014).

Microfluidic devices are characterized by having one or more channels with dimensions typically smaller than 1 mm. Fluids moving through these channels exhibit laminar flow with Reynolds numbers most frequently ranging from 0.1 to 100 (Yager, 2008). The use of these devices can provide several significant advantages in both chemical and physical processes including increased process efficiency, consumption of smaller amounts of fluid and material, better-controlled and safer conditions for chemical reactions, and lower power consumption. Such aspects have in fact been the main motivation for the present study, as part of a wider scope research on the development of a portable demonstration unit for biodiesel continuous synthesis based on microreactors with waste heat reuse. Even though the usual biodiesel synthesis batch process is well established, the process enhancement via microreactors seems to be a promising way to improve the synthesis and reduce residence times (Al-Dhubabian, 2005; Guan et al., 2008; Charoenwat and Dennis, 2009; Wen et al., 2009; Sun et al., 2010; Santaceria et al., 2012; Martinez et al., 2012).

Another key advantage of using microfluidic devices is their often low development and material costs, especially when compared to full-scale high-volume unit operation devices. However, the materials used and microfabrication processes employed to develop these microfluidic tools greatly affect the manner in which flow occurs within the device, and both the materials and the complexity of the microfabrication process can determine whether a particular microfluidic device is viable for large-scale processes.

A variety of materials have been used to manufacture microfluidic devices, such as silicon, metals, ceramics, glasses, and polymers, with silicon being one of the most popular materials used in recent decades (Ali, 2009). Metals are of great interest for the development of microfluidic devices for industrial applications in which durability and heat transfer requirements are high, since metals possess both durability and high thermal conductivity. Common manufacturing techniques for etching microchannels in metals include micromachining, electrical discharge (Ali, 2009), and laser ablation (Chen and Darling, 2012). Microfluidic devices can be constructed entirely from metal in which microchannel patterns are etched onto a metal plate, and another metal plate composed of the same material is used to seal

the device together. There are numerous examples in the literature describing different microfabrication methods used to develop these types of all-metal microfluidic devices, as well as their successful application in various chemical processes. Ali (2009) compared two different microfabrication processes, micro end milling and micro electrical discharge, for microfluidic devices composed entirely of metal or entirely of a polymer, and concluded that the end milling procedure resulted in the formation of burrs on metallic surfaces whereas the micro electrical discharge process was capable of producing high aspect ratio microchannels on metals without forming any burrs. Wen et al. (2009) developed a biodiesel microreactor made of stainless steel with zig-zag patterned microchannels etched on the surface using an electrical discharge process. The reactor was sealed by diffusion bonding. Guerrieri and Naveira-Cotta (2014) built a microchannel heat exchanger to study the cooling and waste heat recovery from high-concentration photovoltaic cells. The microchannels were engraved onto a copper chip, using a micro milling technique and physically sealed with another copper plate using tightening screws.

A significant disadvantage of devices composed entirely of metal, however, is the inability to directly visualize flows within these devices. Thus, a hybrid device, in which microfluidic channels are etched into a metal substrate and then sealed with a glass plate is desirable for visualization and direct observation of flows. For instance, Nascimento et al. (2013) built a metal–glass hybrid heat sink device to experimentally evaluate the flow of boiling R134a in microchannels. The microchannels were etched into a copper plate using a disk saw end mill and the device was sealed with a glass plate with clamping screws.

The sealing of a microfluidic device is an important step in the fabrication process and for all-metal devices this step is usually accomplished by welding, for example, diffusion bonding (Tabeling, 2005), or via physical pressure through the use of screws or clamps (Guerrieri and Naveira-Cotta, 2014). The sealing of microfluidic devices composed of two entirely different materials, like glass and metal, is less common and often more difficult to achieve. However, several methods including anodic bonding (Tabeling, 2005) have been successfully used to seal silicon–glass microfluidic devices.

In this work, we first describe in detail a process for fabricating metal–metal microfluidic devices or metal–glass hybrid devices using a micromachining technique and either a welding or epoxy adhesion sealing method. The advantages of the fabrication method and sealing processes described here are that they involve 1) a simpler process with fewer steps, 2) are inexpensive, and 3) in the case of the metal–glass sealing method, it does not require the high temperatures used for other common metal–glass sealing methods. Then, it is demonstrated that the final products are suitable for use as Y-junction microreactor devices, through results from microscopic characterization and flow and visualization testing experiments. An experimental setup is finally built to test the microreactor for actual biodiesel synthesis, using the metal–metal device and employing soybean vegetable oil, ethanol and so-

dium hydroxide as a catalyst, so as to confirm the reaction enhancement allowed for by the designed microfluidic system.

2. DESIGN OF THE MICROREACTOR

In this paper, Y-junction microfluidic devices were constructed to demonstrate the fabrication process proposed in this work. The devices were composed of a base plate on which the microchannel structure was etched and a cover plate used to hermetically seal the device. Here, the devices were all built with a brass metal base plate and either a metal or glass cover plate. Both the base and cover plates of all devices were rectangular in shape, 20-mm wide, 40-mm long, and 3-mm thick.

The microdevices were designed with a Y-junction microchannel architecture consisting of two entrance channels that converge into a single mixing channel with a length of 395.35 mm. All channels possessed a square cross section of 0.4×0.4 mm. The two inlet and single outlet connections to the exterior were made on the back side of the base plate. Figure 1a shows a schematic drawing of the microfluidic device and Fig. 1b shows the position of the inlet and outlet connections on the external surface of the base plate.

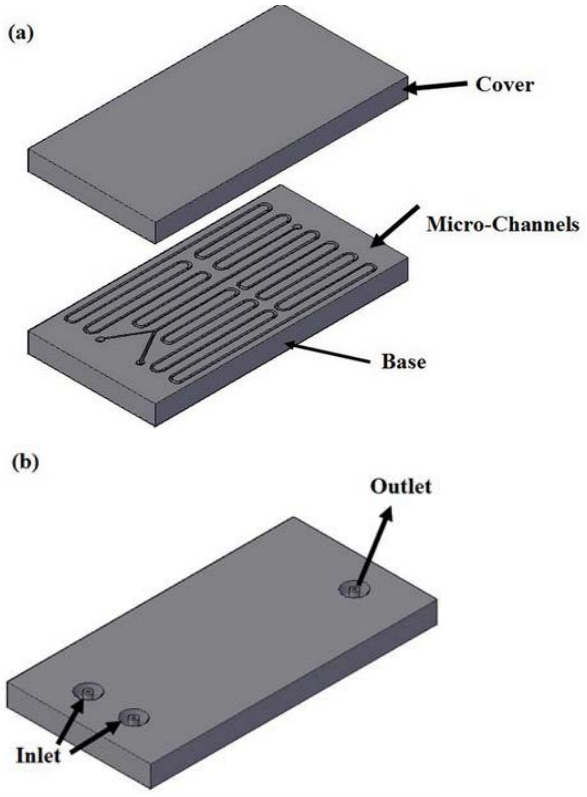

FIG. 1: (a) Schematic drawing of the microreactor; (b) connections to the outside

3. MICROFABRICATION

Micromilling is a flexible machining process that allows the fabrication of high quality microfluidic devices (Ashman et al., 2006). In this work, all microchannels were constructed using a computer numerically controlled (CNC) micromilling device (Micro CNC Minitech Machinery), with a maximum drill rotational speed of 60,000 rpm and a displacement accuracy of 1 μm.

In both cases (metal–metal and metal–glass devices), the fabrication procedure started with the facing step, where a thin layer of material was removed from all surfaces of each plate to ensure the plane's perpendicularity to the rotating axis of the workpiece and uniformity of all substrate surfaces. The layout of the microchannel pattern was designed using AutoCAD 2012 (AutoDesk®) software which could then be directly imported into the device's software MecSoft VisualCAD 2012. The software then uses this design to automatically generate a code (GCODE) that contains the specific sequence of cuts and movements necessary to etch the pattern into the material substrate. The details of the fabrication and sealing process for both cases, metal–metal and metal–glass, are detailed in the next section.

3.1 Metal–Metal Microfluidic Devices

Fabrication of the metal–metal microfluidic devices consisted of four basic steps: 1) preparation of the base and cover plate surfaces, 2) deposition of a thin layer of tin, 3) etching the microchannel pattern on the base plate using micromachining, and 4) finally sealing the two plates together. Figure 2 schematically illustrates these four stages of the fabrication process.

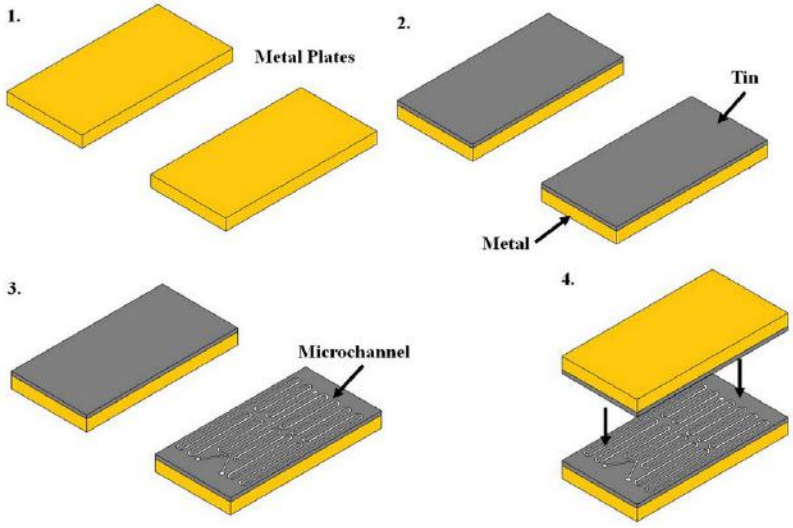

FIG. 2: Schematic representation of the microfabrication process for the metal–metal microdevices: 1) surface preparation; 2) tin deposition on the surface; 3) engraving of the microchannel pattern; 4) sealing of the microsystem

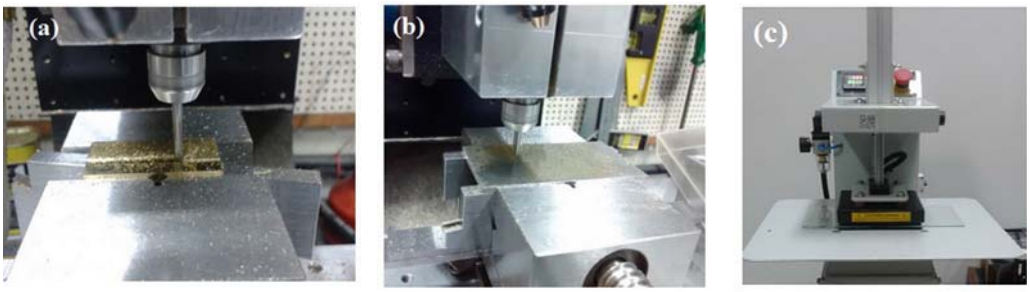

FIG. 3: Machining operations used in the manufacturing of the microfluidic device: a) facing; b) milling operation; c) sealing

In the first stage of the process, preparation of the surfaces, any imperfections on the base and cover plate surfaces were removed in a facing step, using a 3-mm diameter tool bit (Fig. 3a). Although this step could be accomplished through conventional facing tools not intended for microfabrication, this choice in fact aided in a more adequate deposition of a tin layer. In the next step the plates were heated up to 200^{o}C and a thin layer of liquid tin was deposited evenly along the inner surfaces of the plates and allowed to dry. In the third stage, the inlet and outlet holes were drilled and the microchannel pattern was engraved onto the tin surface through a milling process using a 0.4-mm tool bit (Fig. 3b). Finally, to hermetically seal the device base and cover plates were aligned and pressed against each other inside a pneumatic heat press (PLS 150 by Metalnox) set at 85 psi and 230oC for approximately 75 min (Fig. 3c). The plates were then allowed to cool at room temperature while maintaining a pressure of 85 psi. The two plates were effectively sealed due to the annealing of the two thin layers of tin on each of the plates.

Figure 4 shows a single plate (bottom plate) in its various stages of the manufacturing process, as described in Fig. 2. Figure 4a illustrates the metal plate just

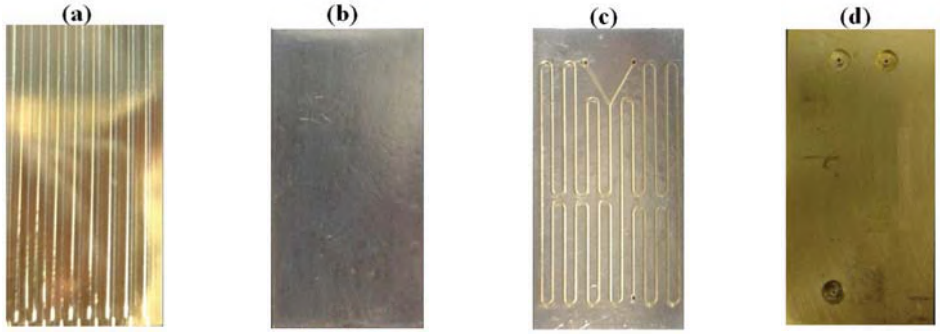

FIG. 4: Fabrication steps for the microdevice: a) metal plate after the facing procedure; b) the surface of the plates with the tin layer; c) the base plate with the microchannel machined onto the tin layer surface; d) the external face with three holes

after the facing step, Fig. 4b illustrates the metal plate after the tin deposition across one of its surfaces, Fig. 4c shows the board after etching microchannels, and Fig. 4d shows the external face of the bottom plate and the details of its three holes.

3.2 Metal–Glass Microfluidic Devices

The process of fabrication of metal–glass microdevices was similar to that of the metal–metal devices and could be divided into three steps: 1) surface preparation of the base plates, 2) etching of a microchannel pattern onto the base plate surface, and 3) sealing the device. Figure 5 schematically illustrates the three steps of the metal–glass device manufacturing process.

Here, the base plate material was also brass, and the metal surface was first prepared in the same way as the plates used for the metal–metal devices (Fig. 3a). After the base plate surface was prepared by facing, a 0.4-mm tool bit was used to etch microchannels onto the surface. Figure 6 shows the base plate with the etched microchannel.

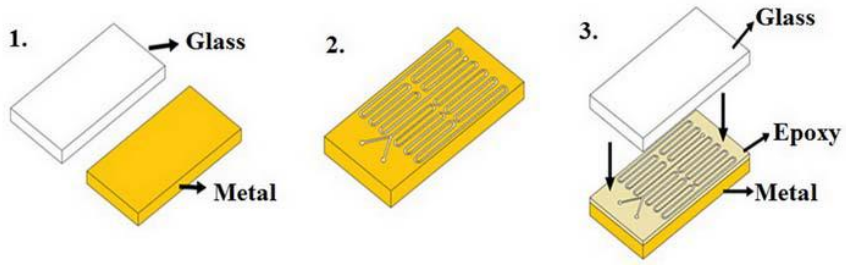

FIG. 5: Schematic representation of the fabrication process for metal–glass microdevices: 1) preparation of the base; 2) engraving of the channels; 3) sealing

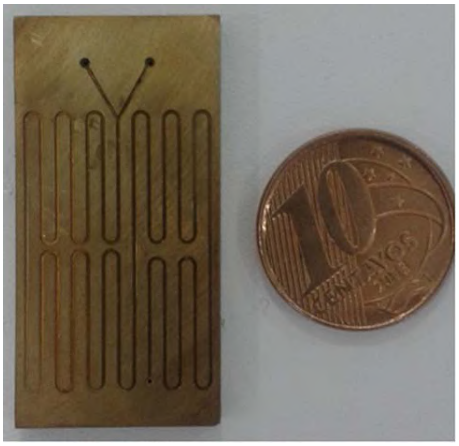

FIG. 6: Microchannels machined onto the surface of a brass base plate

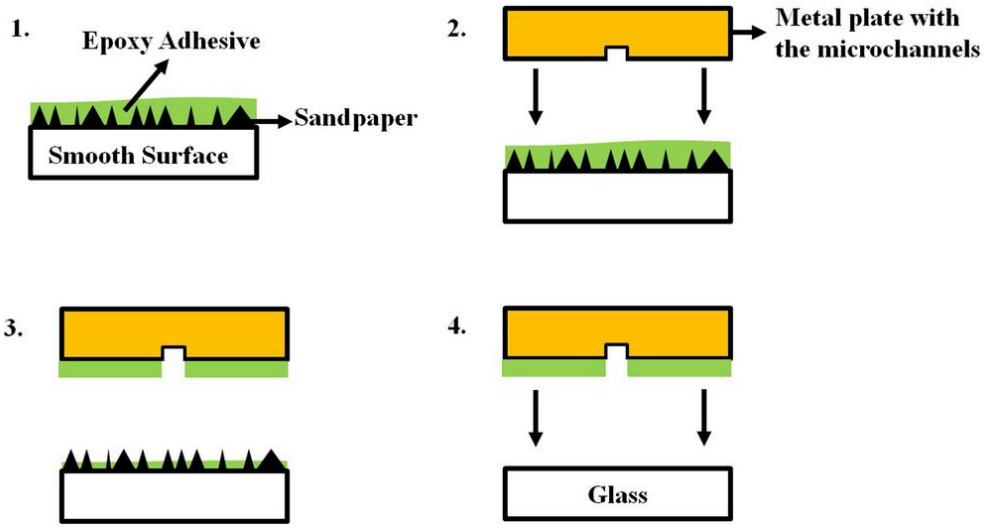

FIG. 7: Scheme of the sealing process for the metal–glass microdevice: 1) spreading of the epoxy adhesive on the surface of the sandpaper; 2) base plate is placed in contact with the epoxy; 3) adhesion of the epoxy to the base plate; 4) sealing of the device with the glass cover plate

The third and final step, the sealing of the device, involved using a two-component epoxy adhesive of polyamide and tertiary amine (POLY HOBBY – PULVITEC) with 2 hours cure time, to seal the plates together. In this step, it was critical to ensure that the epoxy was spread between the two plates in a uniform manner, thus resulting in a uniform seal, and that no epoxy adhesive blocked the channel pathway. Thus, instead of spreading the epoxy directly onto the base plate, a layer of epoxy adhesive was first deposited on a small sheet of sandpaper (600 particles/cm^2 with 25.8-μm average particle diameter), and the brass base was then placed in contact with the sandpaper. The epoxy adhesive is deposited over the sandpaper and then transferred to the metal plate simply by direct contact. The rough surface of the sandpaper impairs the lateral movement of the epoxy, allowing for a uniform transfer of a thin adhesive layer over the brass surface, while avoiding an excess amount of epoxy in any position along the surface. Once the epoxy was transferred onto the brass base, the glass plate was aligned and placed in contact with the base and the epoxy adhesive was allowed to dry for a minimum of 2 h. Figure 7 shows each of the individual steps in the metal–glass device sealing procedure.

Figure 8a–e illustrates the process, first by showing the sandpaper fixed on a flat surface (Fig. 8a), the epoxy adhesive being spread onto the sandpaper (Fig. 8b), the base plate in contact with the epoxy (Fig. 8c), the surface of the sandpaper after removing the base plate (Fig. 8d), and the base plate with the glass cover plate sealed with epoxy (Fig. 8e).

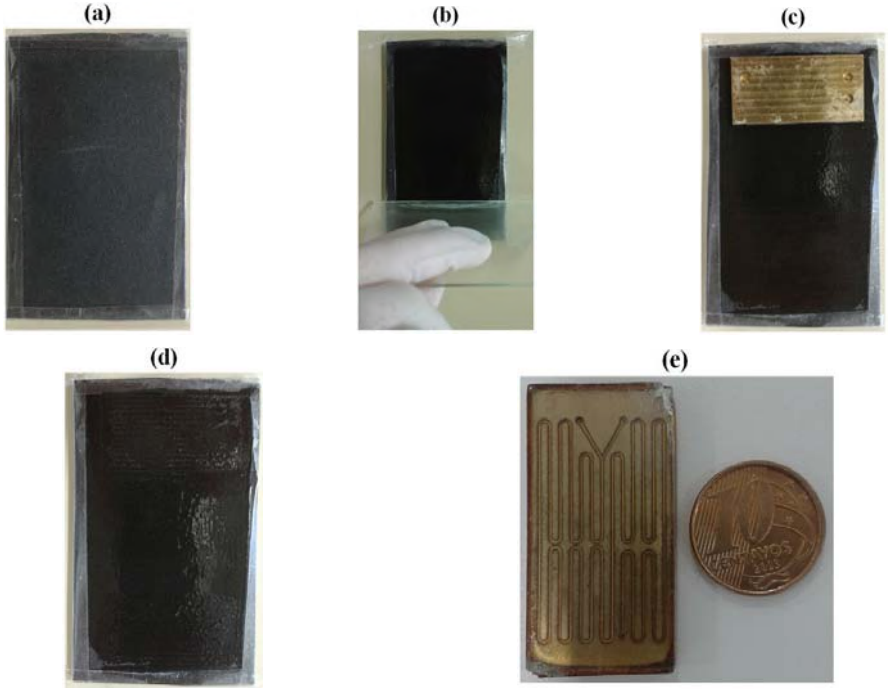

FIG. 8: Steps in the sealing of the metal–glass microdevices: a) sandpaper fixed at uniform surface; b) epoxy being spread on the sandpaper; c) base plate of the micro-channels in contact with the epoxy; d) sandpaper after removing the base plate; e) sealed system

4. CHARACTERIZATION AND TESTING

4.1 Metal–Metal Microdevice

After the microchannel pattern was etched onto the tin covered base plate, microscopic images of various points of the surface were obtained with a 3D Hirox KH-8700 digital microscope for evaluating the machining quality and to quantify the dimensions of the microchannel.

Figure 9a shows the etched microchannel on the surface of the microdevice's base plate. An enlarged image of the region inside the rectangle in Fig. 9a is presented in Fig. 9b. The channel widths of this region were examined and measured, and an example of the 3D images generated, including a profile measurement across the width of the channel, is shown in Fig. 9c. After 40 measurements the mean width of the microchannel was 401 $\pm$ 4 μm, and the mean depth of the microchannel was 396.4 $\pm$ 1.42 μm.

The quality of the seal and final product was verified by cutting the completed device along the dotted line shown in Fig. 10a and examining the cross section of the microchannel. Microscopic images of the cross section were taken to verify the quality of the sealing process and the final dimensions of the microchannels (Fig. 10b).

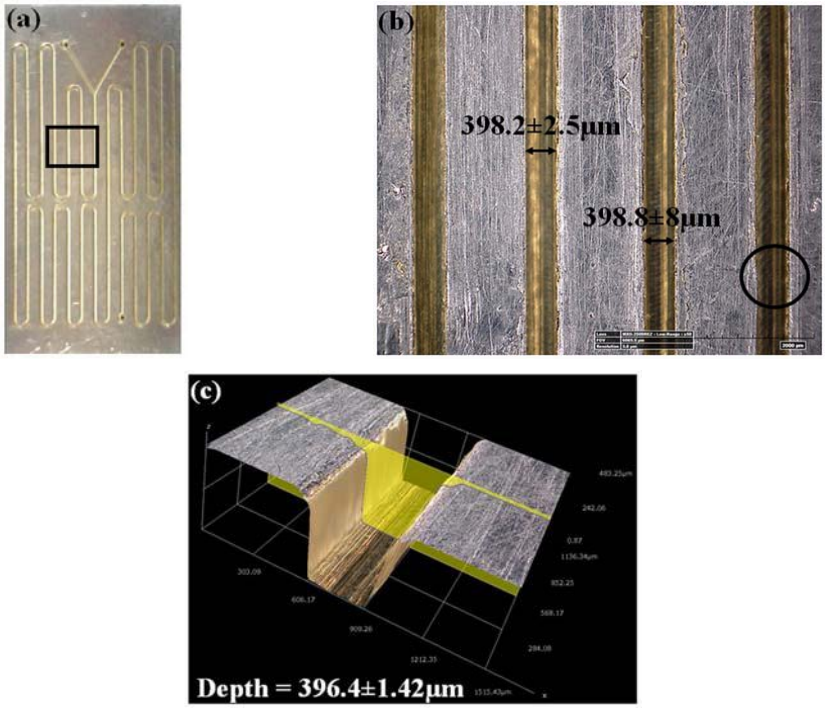

FIG. 9: Microscopic images of microchannels after machining: a) region of microsystem where the dimensions were obtained; b) microscopic image of the square region indicated in (a); c) profile of the depth of the microchannel within the circled region indicated in (b)

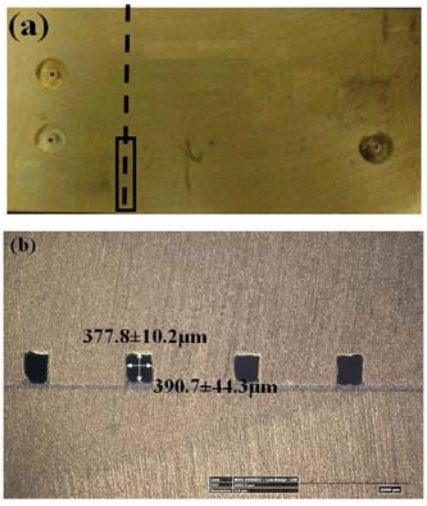

FIG. 10: (a) External image of the sealed device, indicating the region where the device was sectioned and the microscopic images were obtained; (b) microscopic image of the cross section

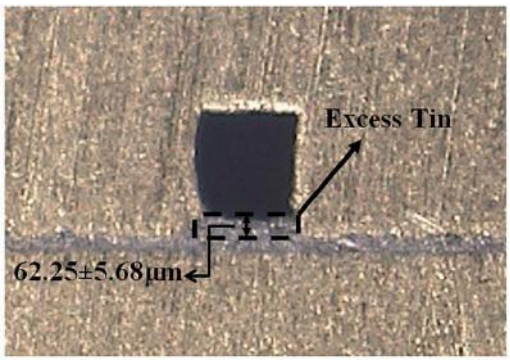

FIG. 11: Enlarged image of the second microchannel of Fig. 10b showing the excess tin at the microchannel wall

After 15 measurements the mean width of the microchannel was 377.8 ± 10.2 μm, and the mean height of the microchannel was 390.7 ± 44.3 μm. This reduction in dimensions is due to the manufacturing and sealing process. There were no observable obstructions blocking the channel and the seal appeared to be complete. In some regions, the height of the microchannel decreased due to excesses of tin (Fig. 11). After four measurements, the mean height of the excess tin was estimated as 62.25 ± 5.68 μm. In the tin layer shown in Fig. 12, four measurements were taken and the mean height of the tin layer was estimated as 44.75 ± 10 μm.

4.2 Biodiesel Synthesis

An experimental setup was designed and built to carry out the biodiesel synthesis in the metal–metal microreactor, and its main components are shown in Fig. 13. The experimental setup is composed of: a microreactor; an electrical resistance made of constantan of 10 Ω, used as a heater so as to analyze the temperature influence in the reaction, combined with a flux meter and a thermocouple; two syringe pumps (NE 1000); a vessel for collecting the end product of the transesterification reaction, immersed in a bath of water with ice which aids in halting the reaction, and thus evaluating the actual efficiency/performance of the microreactor; a source of direct current with controlled voltage; a data acquisition system (Agilent 34970-A), for

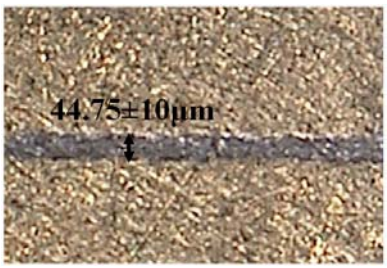

FIG. 12: Detailed image of the interface tin layer

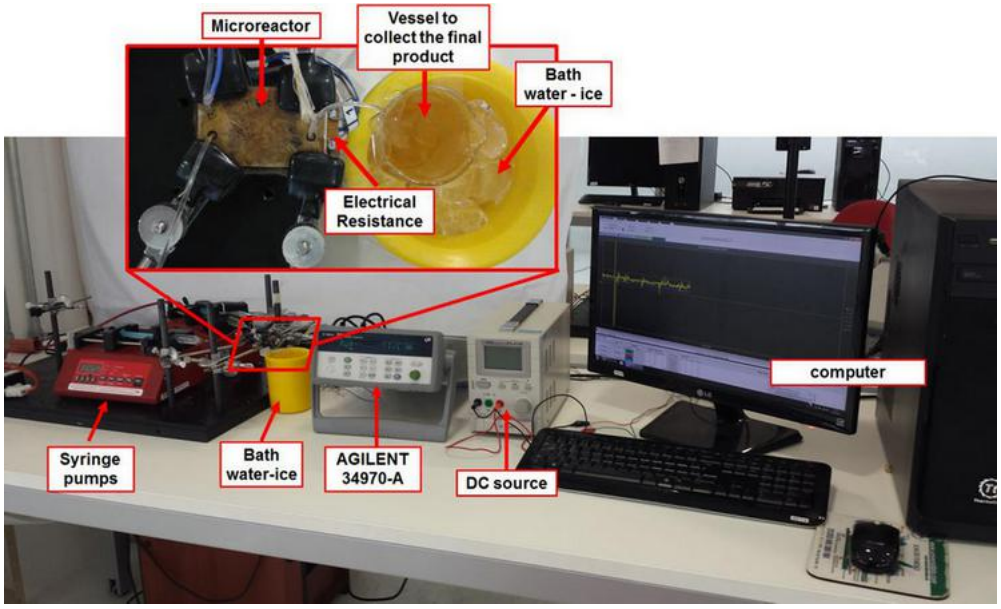

FIG. 13: Experimental setup for biodiesel production in metal–metal microreactor

reading data provided by the thermocouples and flux meter; a computer for data acquisition; and four thermocouples, with two located in each entrance of the microdevice, the other located at the exit of the microdevice and, the last one, measuring the ambient temperature.

In the biodiesel synthesis here illustrated, use was made of soybean vegetable oil of food grade, absolute ethanol (99^{o} GL from B'Herzog) and sodium hydroxide, NaOH, (from Petroquimios) as a catalyst for the reaction. The experimental procedure is initiated by pumping the solution of ethanol with NaOH and the soybean oil to the interior of the microreactor though the two entries. The two streams then enter in contact and the mass transfer process and transesterification reaction occur, mainly by diffusion along the length of 39.5 cm of the microchannel. The final product of the reaction is collected in a vessel immersed in the ice–water bath that serves to halt the reaction and thus allows for the characterization of the microreactor performance. The collected product is separated into two phases, the fatty acid ethyl esters (FAEE) and glycerol, that are washed with distilled water at 75^{o}C, thereby removing the remaining waste catalyst and glycerol.

The analysis of the ethyl esters was made by a high-performance liquid chromatographer (HPLC) from Thermo Scientific, model Ultimate^{TM} 3000, and was also performed on a column from Thermo Scientific, model Acclaim^{TM} 120. Each sample was analyzed three times, and thus three chromatograms were obtained for each sample for statistical evaluation of the measurement procedure. In these chromatograms, the components of each sample, corresponding to the peaks, were identified and the areas of these peaks were obtained using the Chromeleon 6.80 software.

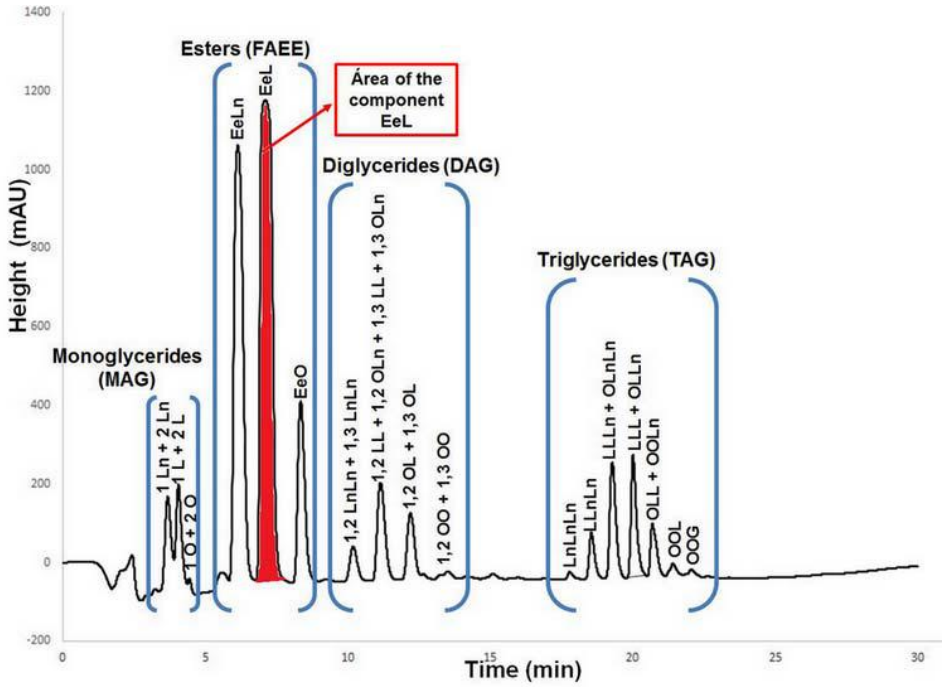

FIG. 14: Chromatogram of a biodiesel sample with the identified components and the corresponding groups

Figure 14 illustrates a typical chromatogram to be analyzed. It is possible to observe both the identification of the components of the biodiesel sample corresponding to peaks, such as the peak of the component Linoleic acid ethyl ester (EeL), as well as the groups (triglycerides, diglycerides, monoglycerides or esters) wherein these components are inserted. In this chromatogram, it is also possible to identify the area occupied by each component. To exemplify, the area identified by the color red corresponds to the area of the component EeL, and, thus as the component EeL, each component will have its respective area.

The quantification of ethyl esters was obtained using Eq. (1) developed by Andrade et al. (2011) for the determination and characterization of FAEE by high-performance liquid chromatography (HPLC):

$$C_{\mathrm{FAEE}} = 100 \times \left(\frac{Ac_{\mathrm{FAEE}}}{Ac_{\mathrm{FAEE}} + Ac_{\mathrm{MAG}} + (2Ac_{\mathrm{DAG}} + (3Ac_{\mathrm{TAG}})} \right), \qquad (1)$$

where *Ac* is the corrected area of each group of components present in the biodiesel sample. This corrected area of each group is determined by the sum of the ratio between the areas of each component (*A*) and the number of double bonds (NDD) of a component, or,

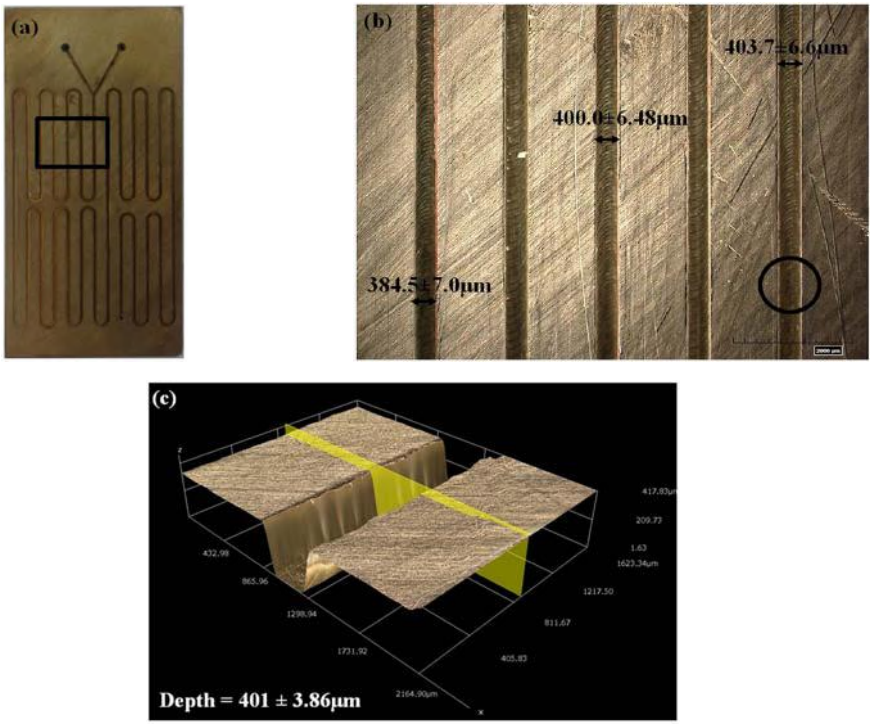

FIG. 15: Microscopic images of the microchannel after machining: a) region of microsystem where the dimensions were obtained; b) microscopic image of the square region indicated in (a); c) profile of the depth of the microchannel of the circled region indicated in (b)

$$Ac_{\mathrm{GROUP}} = \sum \frac{A_{\mathrm{component}}}{\mathrm{NDD}_{\mathrm{component}}} .$$

The yields of fatty acids ethyl esters in biodiesel samples were analyzed for a molar ratio ethanol/oil 20:1, and for a quantity of NaOH catalyst of 1.0 wt.% at a controlled temperature of 47.5oC. A yield of FAEE of 87.2% with 98% of triglyceride conversion has been achieved for a residence time of 10 min. This analysis was not done as yet for an optimized parametric arrangement, but it quite clearly illustrates the applicability potential of such a microreactor in the biodiesel synthesis.

4.3 Metal–Glass Microdevice

The quality of the machining process for the metal–glass microdevice was characterized similarly to that of the metal–metal device. After the microchannel pattern was etched onto the brass base plate, microscopic images were taken at different points along the channel, as shown in Fig. 15a, in order to assess its dimensions and the quality of machining.

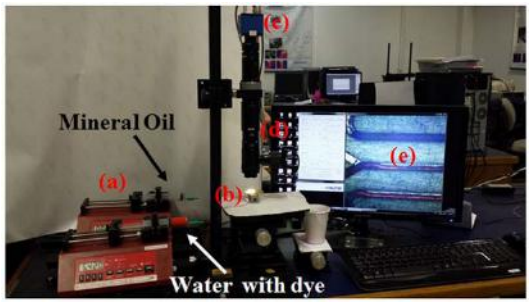

FIG. 16: Experimental setup for metal–glass microdevices testing and flow visualization

Figure 15b,c shows the microscopic images of the estimated mean width and depth, respectively, of the microchannel in the region indicated in Fig. 15a. After 50 measurements, the mean width of the microchannel was 398 ± 11 μm, and the mean depth of the microchannel was 401 ± 3.86 μm, indicating that the channel possessed approximately a square section.

Testing of the sealed microdevices was conducted by pumping a two-phase liquid–liquid system through the microchannels pathway and visually inspecting for possible leaks and for the resulting flow patterns. The experimental setup used for this analysis, shown in Fig. 16, was composed of: (a) two syringe pumps (NE 1000), (b) the metal–glass fabricated microfluidic device, (c) a high-resolution CCD camera (Pixelink PL-H96YACG) connected to (d) a microscope (Navitar High Magnification Imaging – 12X Zoom lenses), and (e) a computer for data acquisition. The working fluids used for the two-phase systems were mineral oil (Sigma-Aldrich-330779) and deionized water with a red dye (Suvinil), wherein 3.6 ml of dye was diluted with 20 ml of deionized water.

The two liquid phases, mineral oil and water with a dye, were pumped simultaneously into the device via separate inlets and brought into direct contact at the end of the Y-junction, marking the beginning of the reacting channel. All flow processes through the microfluidic devices were documented with high-resolution video.

The quality of the device's sealing was tested using two different volumetric flow rates presented in Table 1. The flow rates were adjusted in order to produce different flow patterns, typical of the application as a microreactor for biodiesel production often comprised of a two-phase flow of vegetable oil and alcohol + catalyst. In each case, the flow patterns were closely observed for any possibilities of leakage.

Figures 17 and 18 show the behavior of the two-phase water–oil flow inside the microchannels for the two different flow rates shown in Table 1, respectively, for ex-

TABLE 1: Volumetric flow rates used in the visualization experiments

Experiment	Water with dye, ml/min	Mineral oil, ml/min
1	0.024	0.050
2	0.024	0.150

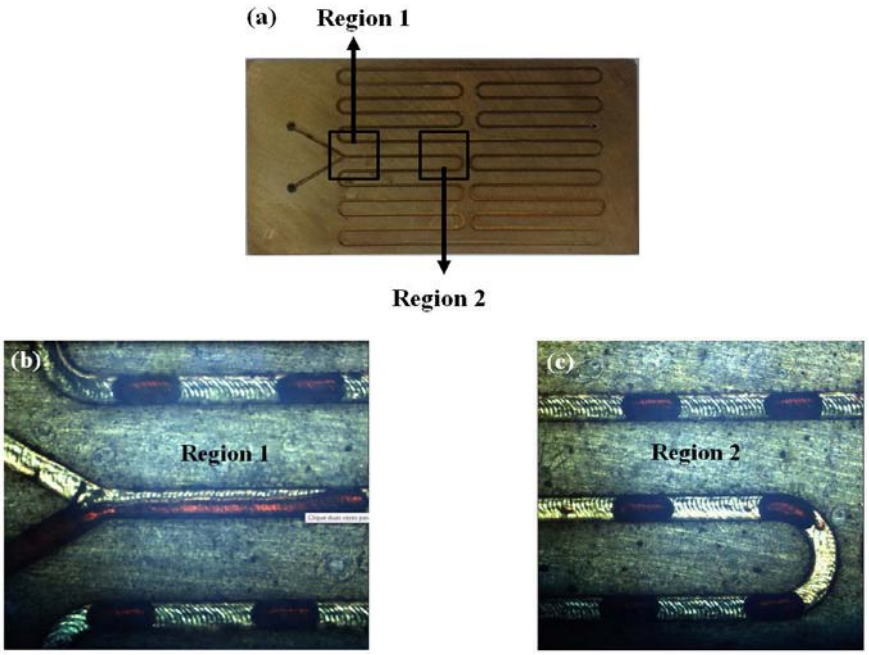

FIG. 17: Microscopic images of the two-phase water–oil flow for experiment 1

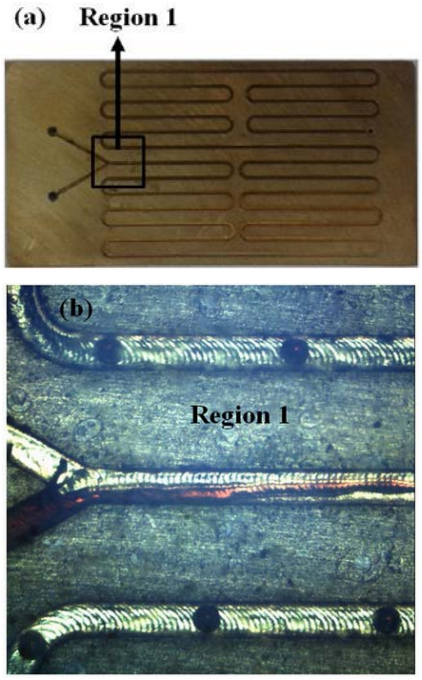

FIG. 18: Microscopic image of the two-phase water–oil flow for experiment 2

periments 1 and 2. In the images shown in both figures, the oil is the continuous phase while the water with a dye is the dispersed phase. As expected, the size of the dispersed aqueous phase plugs (Fig. 17 – Experiment 1) and droplets (Fig. 18 – Experiment 2), decreased as the flow rate of the continuous oil phase increased, while stable monodispersed populations of plugs/droplets were produced. These images, as well as all on-line visual inspection conducted during the experiment, were possible only for the device which used a glass cover plate, hence its advantage over the device constructed entirely from metal for flow characterization purposes.

5. CONCLUSIONS

The present work deals with the design, fabrication, characterization, and testing of microreactors for continuous synthesis of biodiesel, part of the effort in developing a modular portable demonstration unit.

A detailed fabrication process of two types of metallic microreactors is described, one utilizing a metal cover and the other utilizing a glass cover. Microscopic imaging was used to observe the quality of the machined microchannels, and demonstrated that the micromilling process here presented is a suitable technique for microchannel fabrication on a metal substrate. The metal–metal microdevice was sealed via welding using tin as the additional metallic layer. Microscopic observation of the cross sections of the device showed that this technique can be used to make reliable metal–metal sealing of microfluidic devices with a small, manageable amount of distortion to the final channel size and shape. The sealing for the metal–glass microdevice was tested through visual inspection of on-line two phase liquid–liquid flows within the device. Two-phase flow experiments showed that the microfluidic device did not leak under the flow conditions selected and offered the advantage of on-line visual analysis of flows within the device. The metal–metal microreactor was also tested under actual biodiesel synthesis conditions, through a carefully prepared experiment, that already demonstrated an excellent total triglyceride conversion of 98% in 10 min residence time, and served to demonstrate the applicability of this device in the process.

The proposed fabrication technique provides a quick, simple, and economic way to fabricate microfluidic devices for use in industrial applications, such as in the here proposed production of biodiesel, which requires high temperatures, high pressures, relatively high chemical resistance, and in addition, in the case of the metal–glass device, the ability to directly visualize flow processes. More recently, research has been directed towards simulation of microreactors for biodiesel synthesis (Pontes et al., 2015), accounting for both stratified and droplet flow patterns, so as to reach optimized configurations for the final assembly of a modular structure of multiple parallelized microreactors.

ACKNOWLEDGMENTS

The authors would like to acknowledge the financial support provided by the Brazilian government research sponsoring agencies (CNPq, FAPERJ, and ANP PRH).

REFERENCES

Al-Dhubabian, A. A., *Production of Biodiesel from Soybean Oil in a Micro Scale Reactor*, M.Sc. thesis, Oregon State University, Corvallis, OR, USA, 2005.

Ali, M. Y., Fabrication of microfluidic channel using micro end milling and micro electrical discharge milling, *Int. J. Mech. Mater. Eng.*, vol. **4**, pp. 315–322, 2009.

Andrade, D. F., Mazzei, J. L., and d'Avila, L. A., Separation of acylglycerols from biodiesel by high performance liquid chromatography and solid-phase extraction, *Rev. Virtual Quim.*, vol. **3**, no. 6, pp. 452–466, 2011.

Ashman, S. and Kandlikar, S. G., A review of manufacturing processes for microchannel heat exchanger fabrication, *Fourth Int. Conf. on Nanochannels, Microchannels, and Minichannels – ICNMM*, June 19–21, Limerick, Ireland, 2006.

Charoenwat, R. and Dennis, B. H., Transesterification of vegetable oils with a continuous flow capillary reactor, *Proc. ASME 2009 — Early Career Technical Conf.*, Arlington, Texas, USA, 2009.

Chen, H., Li, J., Zhou, W., Pelan, E. G., Stoyanov, S. D., Arnaudov, L. N., and Stone, H. A., Sonication – Microfluidics for fabrication of nanoparticles-stabilized microbubbles, *Langmuir*, vol. **30**, pp. 4262–4266, 2014.

Chen, T. C. and Darling, R. B., in: M. Kahrizi (Ed.), *Fundamentals of Laser Ablation of the Materials Used in Microfluidics, Micromachining Techniques for Fabrication of Micro and Nano Structures*, 2012; ISBN: 978-953-307-906-6, InTech, available from: http://www. intechopen. com/books/ micromachiningtechniques-for-fabrication-of-micro-and-nano-structures/fundamentals-of-laser-ablation-of-the-materials-usedin-microfluiducs.

Chen, Y. H., Kuo, Z. K., and Cheng, C. M., Paper – A potential platform in pharmaceutical development, *Trends Biotechnol.*, vol. **33**, Issue 1, pp. 4–9, 2015.

Correa, M., Guerrieri, D. C., Naveira-Cotta, C. P., and Colman, J., Design and manufacture of microchannel heat sinks for high concentration photovoltaic cells, *22nd Int. Congress of Mechanical Engineering — COBEM*, November 3–7, Ribeirão Preto, São Paulo, Brazil, 2013.

Guan, G., Kusakabe, K., Sakurai, N., and Moriyama, K., Continuous production of biodiesel using a microtube reactor, *Chem. Eng. Trans.*, vol. **14**, pp. 237–244, 2008.

Guerrieri, D. C. and Naveira-Cotta, C. P., Experimental and theoretical analysis of a microchannel heat exchanger for high concentration photovoltaic cells, *14th Int. Symp. on Convective Heat and Mass Transfer*, June 8–13, Turkey, 2014.

Kong, F., Zhang, X., and Hai, M., Microfluidics fabrication of monodisperse biocompatible phospholipid vesicles for encapsulation and delivery of hydrophilic drug or active compound, *Langmuir*, vol. **30**, pp. 3905–3912, 2014.

Le Roux, D. L., Root, B. E., Reedy, C. R., Hickey, J. A., Scott, O. N., Bienvenue, J. M., Landers, J. P., Chassagne, L., and de Mazancourt, P., DNA analysis using an integrated microchip for multiplex PCR amplification and electrophoresis for reference samples, *Anal. Chem.*, vol. **86**, pp. 8192–8199, 2014.

Martinez, E. L., Martins, P. F., Jardini, A. L., Gutierrez-Rivera, L., and Filho, R. M., Continuous synthesis and in situ monitoring of biodiesel prouction in different microfluidic devices, *Ind. Eng. Chem. Res.*, vol. **51**, pp. 10755–10767, 2012.

Nascimento, F. J., Leao, H. L. S. L., and Ribatski, G., An experimental study on flow boiling heat transfer of R134a in a microchannel-based heat sink, *Exp. Thermal Fluid Sci.*, vol. **45**, pp. 117–127, 2013.

Nilsson, M. A., Kulkarni, R., Gerberich, L., Hammond, R., Singh, R., Baumhoff, E., and Rothstein, J. P., Effect of fluid rheology on enhanced oil recovery in a microfluidic sandstone device, *J. Non-Newtonian Fluid Mech*., vol. **202**, pp. 112–119, 2013.

Pontes, P. C., Naveira-Cotta, C. P., Macedo, E. N., and Quaresm, J. N. N., Integral transforms analysis of three-dimensional mass transfer in the transesterification process in microreactors, *Proc. 7th Int. Symp. on Advances in Computational Hea Transfer, CHT-15*, ICHMT, 24–29 May, Piscataway, USA, 2015.

Santaceria, E., Di Serio, M., Tesser, R., Turco, R., Tortorelli, M., and Russo, V., Biodiesel process intensification in a very simple microchannel device, *Chem. Eng. Process.*, vol. **52**, pp. 47–54, 2012.

Sun, P., Wang, B., Yao, J., Zhang, L., and Xu, N., Fast synthesis of biodiesel at high throughput in microstructured reactors, *Ind. Eng. Chem. Res*., vol. **49**, pp. 1259–1264, 2010.

Tabeling, P., *Introduction to Microfluidics*, New York: Oxford University Press, 2005.

Wen, Z., Yu, X., Tu, S., Yan, J., and Dahlquist, E., Intensification of biodiesel synthesis using zigzag micro-channel reactors, *J. Bioresource Technol.*, vol. **100**, pp. 3054–3060, 2009.

Xu, K., Tostado, C. P., Xu, J. H., Lu, Y. C., and Luo, G. S., Direct measurement of the differential pressure during drop formation in a co-flow microfluidic device, *Lab Chip*, vol. **14**, pp. 1357–1366, 2014.

Yager, P., *Basic Microfluidic Concepts*, 2008; http://faculty.washington.edu/yagerp/microfluidicstutorial/basicconcepts/basicconcepts.htm.